On the use of the Lambert function in solving non-Newtonian flow problems

Rafaella Pitsillou
Department of Physics, University of Cyprus, P.O. Box 20537, 1678 Nicosia, Cyprus
E-mail: pitsillou.rafaella@ucy.ac.cy

Georgios C. Georgiou*
Department of Mathematics and Statistics, University of Cyprus, PO Box 20537, 1678 Nicosia, Cyprus
* Corresponding author (georgios@ucy.ac.cy, Tel. +35722892612)

Raja R. Huilgol
College of Science and Engineering, Flinders University, GPO Box 2100, Adelaide SA 5001, Australia
E-mail: rrhuilgol@gmail.com

Abstract

We consider unidirectional flows of ideal or regularized Bingham fluids as well as of viscoelastic fluids for which analytical solutions can be derived in terms of the Lambert W function. Explicit expressions are derived for the radius of the yielded region in partially-yielded circular and axial Couette flows. Analytical solutions are also derived for the velocity and the volumetric flow rate in plane and axisymmetric Poiseuille flow of a Windhab fluid, which is a combination of the Bingham and Papanastasiou models, and for the shear stress in plane Couette flow of an exponential Phan-Thien-Tanner fluid. Finally, the Lambert function is used to solve the Poiseuille flow of a power-law fluid and the Newtonian circular Couette flow with wall slip with non-zero slip yield stress by means of a regularized slip equation, which is valid for any value of the wall shear stress.

Keywords: Lambert function; Poiseuille flow; Couette flow; Bingham plastic; Papanastasiou regularization; Windhab model; Phan-Thien-Tanner model; Wall slip; Slip yield stress.

1. Introduction

The Lambert function $W(x)$ is defined for $x \geq -1/e$ as the inverse of (Corless et al., 1996)

$$y = xe^{x} \quad \Leftrightarrow \quad x = W(x)e^{W(x)} \tag{1}$$

and is multi-valued in the interval $[-1/e, 0)$. More specifically, it consists of two branches, the principal branch denoted by $W(x)$ or $W_0(x)$, for $x \in [-1/e, \infty)$ and the secondary branch, denoted by $W_{-1}(x)$, for $x \in [-1/e, 0)$. The principal branch is strictly increasing from -1 to infinity, while the secondary branch decreases to minus infinity.

The definition of the Lambert function and its implementation in standard packages, such as MATLAB and Mathematica, allows the derivation and subsequent use of analytical solutions of certain non-linear equations. Since the seminal paper of Corless et al. (1996), the W function has been used in deriving analytical solutions of problems in various fields, in science and engineering, including Newtonian and non-Newtonian fluid mechanics (see Pitsillou et al. (2020) and references therein). Below, we summarize the solutions for certain equations encountered in the following sections (see Pitsillou et al., 2020 for the derivations):

$$\ln y + Ay = B, \quad A \neq 0 \quad \Rightarrow \quad y = \frac{1}{A} W(Ae^B) = \frac{1}{A} e^{B - W(Ae^B)} \tag{2}$$

$$y \ln y + Ay = B \quad \Rightarrow \quad y = B / W(Be^A) = e^{W(Be^A) - A} \tag{3}$$

and

$$Ay + B = \ln(Cy + D), \quad A, B \neq 0 \quad \Rightarrow \quad y = -\frac{1}{A} W\left(-\frac{A}{C} e^{B - AD/C} \right) - \frac{D}{C} \tag{4}$$

This paper is concerned with the use of the Lambert W function in solving non-Newtonian flow problems. The first class of materials we consider is that of the viscoplastic or yield-stress fluids, i.e. of materials that flow only if this critical stress is exceeded. A good number of materials exhibiting yield stress, such as pastes, suspensions, gels, and slurries, are of importance in industrial applications, e.g. in food processing, oil-drilling and transport, cosmetics, and in physiological and geophysical flows (Bonn et al., 2017). The most commonly used constitutive equation is that proposed by Bingham (1922), the scalar form of which is as follows:

$$\begin{cases} \dot{\gamma} = 0, & \tau \leq \tau_0 \\ \tau = \tau_0 + \mu \dot{\gamma}, & \tau > \tau_0 \end{cases} \tag{5}$$

where τ is the shear stress, $\dot{\gamma}$ is the shear rate, μ is the plastic viscosity and τ_0 is the yield stress. Equation (5) consists of two branches, which apply to the unyielded ($\tau \leq \tau_0$) and yielded ($\tau > \tau_0$) regions of the flow. The determination of yielded and unyielded regions in viscoplastic flows is a difficult task, especially in two and three dimensions. In order to eliminate the need of determining these regions in the flow domain, Papanastasiou (1987) proposed the following regularized model

$$\tau = \tau_0 \left(1 - e^{-m\dot{\gamma}}\right) + \mu \dot{\gamma} \tag{6}$$

where m is the regularization parameter or stress growth exponent. Equation (6) applies throughout the flow domain, replacing unyielded regions with regions of very high viscosity and eliminating yield surfaces and the need to find them. It approximates the Bingham-plastic model (5) for sufficiently large values of the parameter *m* and is easier to implement. The advantages and disadvantages of the regularization approach have been reviewed by Balmforth et al. (2014).

You et al. (2008) demonstrated that Eq. (6) can be solved for $\dot{\gamma}$ by means of Lambert's W function. Equation (6) can also be put in the aforementioned form $Ay + B = \ln(Cy + D)$. It is easily verified that

$$\dot{\gamma} = \frac{\tau - \tau_0}{\mu} + \frac{1}{m} W\left[\frac{m\tau_0}{\mu} e^{-m(\tau - \tau_0)/\mu} \right] \tag{7}$$

which is reduced to Eq. (5) when $m \to \infty$. You et al. (2008) derived analytical solutions for the planar and axisymmetric Poiseuille flows and pointed out that circular Couette flow requires a numerical solution. They concluded that the Papanastasiou model approximates the behavior of the Bingham fluid very closely (provided that the regularization parameter is sufficiently large).

A constitutive equation combining the Bingham and the Papanastasiou models is the Windhab model, which is recommended for describing the rheological behavior of liquid chocolate for shear rates in the range between 2 and 50 s^{-1} (Figura and Texeira, 2007). This can be written as follows:

$$\tau = \tau_0 + \mu \dot{\gamma} + (\tau_1 - \tau_0)\left(1 - e^{-\dot{\gamma}/\dot{\gamma}^*}\right), \quad \tau > \tau_1 \tag{8}$$

where τ_0 is the (initial) yield stress, $\tau_1 \geq \tau_0$ is the extrapolated (or 'hypothetical') yield stress, and $\dot{\gamma}^*$ is a critical shear rate below which the model applies (instead of the ideal Bingham-plastic model). This critical value corresponds to a maximum of the shear-induced loss of structure (Figura and Texeira, 2007). The corresponding stress is given by

$$\tau^* = \tau_0 + \mu\dot{\gamma}^* + (\tau_1 - \tau_0)\left(1 - \frac{1}{e}\right) \approx \tau_0 + (\tau_1 - \tau_0)\left(1 - \frac{1}{e}\right) \tag{9}$$

The Bingham-plastic model is recovered from Eq. (9) by setting $\tau_1 = \tau_0$ while the Papanastasiou model is obtained when $\tau_0 = 0$ with τ_1 serving as the apparent yield stress of the material and the regularization parameter given by $m = 1/\dot{\gamma}^*$. Glicerina et al. (2016) employed the Papanastasiou model ($\tau_0 = 0$) to fit their rheological data on white chocolate.

Lambert's W function also appears in solutions of other non-Newtonian flows. Syrakos et al. (2016) showed that in the case of partially-yielded annular Couette flow of an ideal Bingham plastic, an explicit closed form expression can be derived for the yield radius in terms of W. A solution of a viscoelastic flow involving W has also been reported by Ferrás et al. (2012) for the plane Couette flow of an exponential Phan-Thien-Tanner fluid.

It is well established that slip may occur in confined flows of complex fluids when the wall shear stress exceeds a critical value τ_c, which is called the slip yield stress (Malkin and Patlazhan, 2018). Spikes and Granick (2003) proposed the following two-branch slip equation

$$\begin{cases} u_w = 0, & \tau_w \leq \tau_c \\ \tau_w = \tau_c + \beta u_w, & \tau_w > \tau_c \end{cases} \tag{10}$$

where τ_w is the wall shear stress, u_w is the slip velocity, i.e. the relative velocity of the fluid respect to that of the wall, and β is the slip coefficient. The value of the latter parameter is a function of the temperature, the normal stress and pressure, and the fluid/wall-interface properties (Damianou et al., 2019). When the slip yield stress τ_c is zero, Eq. (10) is reduced to the classical Navier slip condition (Navier, 1827). Equation (10) and its power-law generalization were used to describe experimental data on Carbopol gels (Piau, 2007) and on hard-sphere colloid suspensions (Ballesta et al., 2012). For a review on experimental values of the slip yield stress the reader is referred to Damianou et al. (2019).

Spikes and Granick (2003) noted that the slip yield stress may be attributed to a combination of chain debonding and disentanglement in the case of polymer flow and that it can also be justified by the slip model proposed by de Gennes (2002) according to which small gas droplets which collect preferentially at nonwetted surfaces are transformed into an extended thin film due to liquid strain. Meeker et al. (2004) proposed a slip mechanism based on elastohydrodynamic lubrication between the squeezed particles and the shearing surface to explain experimental observations. In his review paper, Sochi (2011) notes that the critical shear stress at which slip initiates characterizes the fluid-solid system under the existing physical conditions.

The analogy of Eq. (10) with the two-branch Bingham-plastic constitutive equation (5) is obvious. One needs to determine the parts of the boundary where the no-slip condition applies ($\tau_w \leq \tau_c$) or not ($\tau_w > \tau_c$). For instance, in 1D unidirectional pressure-driven flows, one observes different flow regimes as the pressure drop per

unit length is increased (Kaoullas and Georgiou, 2013). Below a certain critical value there is no slip at all; above that value slip may occur. In 2D unidirectional pressure-driven flow problems there is no slip below a critical value of the pressure gradient, then partial slip occurs along the boundary, and above a second critical pressure gradient (non-uniform) slip occurs along the entire boundary. Determining the parts of the boundary where slip applies or not becomes more difficult in time-dependent flows as these parts evolve with time. For example, in cessation flows slip may occur only initially and cease at a critical time (Damianou et al., 2014; Damianou et al., 2016).

Damianou et al. (2014) employed a regularized version of Eq. (10) in order to eliminate the need of determining the regions of the boundary where slip or no-slip applies, which is of the same form as the Papanastasiou equation:

$$\tau_w = \tau_c \left(1 - e^{-m_c u_w}\right) + \beta u_w \tag{11}$$

where m_c is a growth parameter, which should be large enough so that the behaviour or Eq. (10) is approximated. Equation (11) has been applied in solving numerically both 1D and 2D time-dependent flows of Newtonian and Bingham plastic fluids (Damianou et al., 2014; 2016). Given the analogy with the Papanastasiou equation (6), one can explicitly express the slip velocity as a function of the wall shear stress by means of the Lambert function:

$$u_w = \frac{\tau_w - \tau_c}{\beta} + \frac{1}{m_c} W\left[\frac{m_c \tau_c}{\beta} e^{-m_c(\tau_w - \tau_c)/\beta}\right] \tag{12}$$

The objective of the present work is to review existing and derive new solutions of non-Newtonian flows involving Lambert's W. In Section 2 we consider the circular and annular Couette flows of a Bingham plastic and derive analytical expressions for the yield radii when the material is partially yielded. It is demonstrated that different branches of the Lambert function are used for these two cases. In Section 3, the solutions of You et al. (2008) for the plane and axisymmetric Poiseuille flows of a Papanastasiou fluid are extended to the annular Poiseuille flow and to the more general Windhab fluid. A use of W with a structural thixotropic model is also illustrated. In Section 4, we briefly explain how the shear stress in the plane Couette flow of an exponential PTT fluid is expressed as a function of the moving plate velocity by means of the Lambert function, following Ferrás et al. (2012). In Section 5, Lambert's function is employed to analyse the Poiseuille flow of a power-law fluid as well as the Newtonian circular Couette flow with wall slip and non-zero slip yield stress using a regularized slip equation. We derive an explicit expression for the slip velocity which applies also in the no-slip regime provided that the value of the regularization parameter is sufficiently high. Finally, some concluding remarks are provided in Section 6.

2. Bingham flows

In this section we consider the circular and annular Couette flows of an ideal Bingham plastic and show that in the case where the flow is partially yielded, Lambert's W function can be employed to derive explicit expressions for the radius of the yielded region. Moreover, we show that W can also be applied in a structural thixotropic model for a yield-stress fluid.

2.1 Circular Couette flow

The analytical solution of circular Couette flow of a Bingham plastic with no slip at the wall has been derived by Bird et al. (1983). Since then, various extensions have been reported (See Damianou et al., 2019, and references therein). For example, Chatzimina et al. (2009) derived analytical solutions for a Herschel-Bulkley fluid for certain values of the power-law exponent. More recently, Damianou et al. (2019) derived the solutions for Bingham-plastic flow in the presence of Navier slip or slip with slip yield stress.

We consider the Couette flow of a Bingham plastic between two long, coaxial cylinders of radii R_1 and R_2 ($R_2 > R_1$) assuming that the inner cylinder rotates at a constant angular velocity Ω while the outer one is fixed. In steady state, the θ-momentum equation becomes

$$\tau_{r\theta} = -\frac{c}{r^2} \tag{13}$$

where c is an integration constant. Since the stress $\tau = |\tau_{r\theta}|$ decreases with r, it is clear that below a critical value of the angular velocity only the fluid close to the rotating cylinder is yielded. For convenience, we scale r by R_1, the velocity by ΩR_1, and stresses by the yield stress τ_0 and avoid introducing new symbols for the dimensionless variables. When the fluid between the two cylinders is partially yielded the velocity is given by

$$u_\theta(r) = \begin{cases} r\left[1 - Bn\left\{\dfrac{r_0^2}{2}\left(1-\dfrac{1}{r^2}\right) - \ln r\right\}\right], & 1 \le r \le r_0 \\ 0, & r_0 \le r \le \kappa' \end{cases} \tag{14}$$

where $Bn \equiv \tau_0 / (\mu\Omega)$ is the Bingham number, $\kappa' \equiv R_2 / R_1$ is the radii ratio, and r_0 is the yield radius, which is a root of the following equation (Chatzimina et al., 2009):

$$r_0^2 - 2\ln r_0 = 2/Bn + 1 \tag{15}$$

The above solution applies also to the case where there is no outer cylinder, i.e. to the flow where a cylinder is rotating in an infinite pool of a Bingham fluid. The critical Bingham number, Bn_c, at which the flow is fully yielded corresponds to $r_0 = \kappa'$ and therefore $Bn_c = 2/(\kappa'^2 - 2\ln\kappa' - 1)$. For $Bn \le Bn_c$, the velocity is given by

$$u_\theta(r) = r\left[1 + Bn\left\{\ln r - \frac{2\kappa'^2(\ln\kappa' + Bn^{-1})}{\kappa'^2 - 1}\left(1 - \frac{1}{r^2}\right)\right\}\right] \tag{16}$$

which holds in the entire flow domain. Lambert's W function can be employed to calculate the yield radius as a function of the Bingham number. This solution is easily derived from Eq. (15) (which is of the form $\ln y + Ay = B$):

$$r_0 = \sqrt{-W_{-1}(-e^{-1-2Bn^{-1}})} \tag{17}$$

The '-1' subscript indicates that in this particular solution, the secondary branch of the Lambert function should be used.

2.2 Annular Couette flow

The annular Couette flow was solved by Bird et al. (1983) and has been analyzed in detail by Syrakos et al. (2016). It is briefly outlined here for comparison purposes with the circular Couette flow solution. We consider the same geometry as in the circular Couette flow with the inner cylinder moving in the axial direction at a constant velocity V while the outer one is kept stationary. From the z-momentum equation one finds that

$$\tau_{rz} = -\frac{c}{r} \tag{18}$$

The flow is partially yielded when the speed of the inner cylinder is below a critical value. Using similar scales as above and scaling the axial velocity by V we find that in the partially yielded regime the velocity is given by

$$u_z(r) = \begin{cases} 1 + Bn(r - 1 - r_0 \ln r), & 1 \le r \le r_0 \\ 0, & r_0 \le r \le \kappa' \end{cases} \tag{19}$$

where the Bingham number is now defined by $Bn \equiv \tau_0 R_1 / (\mu V)$ and r_0 is the root of

$$r_0 \ln r_0 - r_0 = 1/Bn - 1 \tag{20}$$

The critical Bingham number at which the flow is fully yielded is $Bn_c = 1/(1 - \kappa' + \kappa' \ln \kappa')$. When $Bn < Bn_c$ the velocity is given by

$$u_\theta(r) = 1 + Bn(r - 1) - \frac{1 + Bn(\kappa' - 1)}{\ln \kappa'} \ln r \tag{21}$$

Equation (20) is of the form (2) and thus it can be solved for r_0 in terms of Lambert's W function:

$$r_0 = e^{W_0\left[(Bn^{-1} - 1)/e\right] + 1} \tag{22}$$

The above solution has been derived in Syrakos et al. (2016). A similar expression has been reported by Férec et al. (2017) who analysed the flow of a Bingham fluid around a rigid rod using the cell model approach. Unlike the corresponding solution for the circular Couette flow, in this case the principal branch of the Lambert function is employed. The predictions of Eqs. (17) and (22) are compared in Fig. 1.

2.3 A structural thixotropic model

In this subsection we provide an instructive example where Lambert's W function may be applied in a non-Newtonian flow problem by simply using the definition (1). Alexandrou et al. (2013) proposed a structural thixotropic model for semisolid slurries, which is based on the Bingham model. In the proposed model, the yield stress is assumed to vary linearly with the dimensionless structural parameter λ, i.e. $\tau_0(t) = \tau_y \lambda(t)$, where t is the time and τ_y is the yield stress of the material when this is fully structured ($\lambda = 1$). The structural parameter has been assumed to follow the following dimensionless first-order rate equation

$$\frac{D\lambda}{Dt} = a(1 - \lambda) - b\lambda\dot{\gamma} e^{c\dot{\gamma}} \tag{23}$$

where $\dot{\gamma}$ is the dimensionless magnitude of the rate of strain tensor (i.e. the shear rate in 1D flows), and a, b and c are positive dimensionless parameters. The two terms in the RHS of Eq. (23) represent the recovery and breakdown rates. At equilibrium, $D\lambda/Dt = 0$ and one finds the corresponding value of the structural parameter

$$\lambda_e = \frac{1}{1 + \frac{b}{a}\dot{\gamma}_e e^{c\dot{\gamma}_e}} \tag{24}$$

Rearranging the above expression and using the definition (1) of W, one gets:

$$\dot{\gamma}_e = \frac{1}{c} W\left[\frac{ca}{b}\left(1/\lambda_e - 1\right)\right] \tag{25}$$

3. Papanastasiou and Windhab flows

In this section, the solution derived by You et al. (2008) for the Papanastasiou fluid is extended to the more general flow of a Windhab fluid. We consider the axisymmetric Poiseuille flow of a Windhab fluid, i.e. the one-dimensional steady, pressure-driven flow in a long cylindrical tube of constant radius R. Given that the shear stress τ_{rz} vanishes at the axis of symmetry, this is given by

$$\tau_{rz} = -\frac{G}{2} r \tag{26}$$

where G is the imposed pressure gradient. With a yield-stress fluid, there is no flow when $G \le 2\tau_0 / R$. When $G > 2\tau_0 / R$, the material yields only in a region close to the wall, i.e. for $r_0 \le r \le R$, where Eq. (8) applies. The yield radius r_0 is given by

$$r_0 = \frac{2\tau_0}{G} \tag{27}$$

For $0 \le r \le r_0$ the material is unyielded, that is the velocity derivative is zero and the velocity is uniform.

We de-dimensionalize the governing equations, scaling lengths by R, stresses by $GR/2$, and the velocity by $GR^2/(2\mu)$. The resulting dimensionless form of Eq. (8) is

$$\tau = Bn + \dot{\gamma} + (B_1 - Bn)\left(1 - e^{-m\dot{\gamma}}\right) \tag{28}$$

where

$$Bn \equiv \frac{2\tau_0}{GR}, \quad B_1 \equiv \frac{2\tau_1}{GR}, \text{ and } m \equiv \frac{GR}{2\mu\dot{\gamma}^*} \tag{29}$$

are respectively the Bingham number, the extrapolated Bingham number, and the dimensionless regularization parameter. With these scalings the yield point coincides with the Bingham number, i.e. $r_0 = Bn$, and Eq. (28) can be rearranged as follows:

$$m\dot{\gamma} = -\ln\left[\frac{1}{1 - Bn/B_1}\left(1 - \frac{\tau}{B_1} + \frac{\dot{\gamma}}{B_1}\right)\right] \tag{30}$$

Solving for $\dot{\gamma}$ in terms of Lambert's W function, one gets

$$\dot{\gamma} = \frac{1}{m} W\left[m(B_1 - Bn)e^{m(B_1 - \tau)}\right] - B_1 + \tau \tag{31}$$

When $Bn = 0$, the above solution is reduced to the expression derived by You et al. (2008) for the Papanastasiou regularized constitutive equation. It is easily verified that when $\tau = Bn$ the shear rate vanishes:

$$\dot{\gamma} = \frac{1}{m} W\left[m(B_1 - Bn)e^{m(B_1 - Bn)}\right] - B_1 + Bn = \frac{1}{m} m(B_1 - Bn) - B_1 + Bn = 0 \tag{32}$$

where the identity $W(xe^x) = x$ has been used. Given that the argument of W in Eq. (31) is always positive, only the primary branch of the Lambert function is involved.

Given that $\dot{\gamma} = -du/dr$ and the dimensionless form of Eq. (26) is $\tau_{rz} = -r$, $\tau = r$ and thus from Eq.(31) we have

$$\frac{du}{dr} = B_1 - r - \frac{1}{m} W\left[m(B_1 - Bn)e^{m(B_1 - r)}\right] \tag{33}$$

Integrating we have

$$u = B_1 r - \frac{r^2}{2} - \frac{1}{m}\int_0^r W\left[m(B_1 - Bn)e^{m(B_1-\xi)}\right]d\xi + D \tag{34}$$

where D is the integration constant. Next, we use the following identity

$$\int W^k(\alpha e^{\beta\xi+\delta})\,d\xi = \frac{1}{k\beta}W^k(\alpha e^{\beta\xi+\delta}) + \frac{1}{(k+1)\beta}W^{k+1}(\alpha e^{\beta\xi+\delta}), \quad k = 1, 2, \cdots \tag{35}$$

which generalizes two identities provided by You et al. (2008). By means of (35) it is easily shown that

$$\int_0^r W\left[m(B_1 - Bn)e^{m(B_1-\xi)}\right]d\xi = -\frac{1}{m}f(r) - \frac{1}{2m}f^2(r) \tag{36}$$

where

$$f(r) = W\left[m(B_1 - Bn)e^{m(B_1-r)}\right] \tag{37}$$

Hence,

$$u = B_1 r - \frac{r^2}{2} + \frac{1}{m^2}\left[\frac{1}{2}f^2(r) + f(r)\right] + D \tag{38}$$

Applying the no-slip condition at the wall, $u(1) = 0$, one finds that

$$D = -B_1 + \frac{1}{2} - \frac{1}{m^2}\left[\frac{1}{2}f^2(1) + f(1)\right] \tag{39}$$

The dimensionless velocity profile thus reads

$$u = \begin{cases} \frac{1}{2}(1 - Bn^2) - B_1(1 - Bn) + \frac{1}{m^2}\left[\frac{1}{2}f^2(Bn) + f(Bn) - \frac{1}{2}f^2(1) - f(1)\right], & 0 \le r \le Bn \\ \frac{1}{2}(1 - r^2) - B_1(1 - r) + \frac{1}{m^2}\left[\frac{1}{2}f^2(r) + f(r) - \frac{1}{2}f^2(1) - f(1)\right], & Bn \le r \le 1 \end{cases} \tag{40}$$

It should be noted that $f(Bn) = m(B_1 - Bn)$. Setting $Bn = 0$ leads to the solution derived by You et al. (2008) for the Papanastasiou model, who also indicated that $f(1)$ terms may be omitted without loss of accuracy.

The volumetric flow rate, which is equivalent to the dimensionless mean velocity in the tube, can be calculated as follows

$$Q = 2\int_0^{Bn} u(Bn)r\,dr + 2\int_{Bn}^1 u(r)r\,dr \quad \Rightarrow \tag{41}$$

$$\begin{aligned} Q = {} & \frac{1}{4}\left(1 - Bn^4\right) - \frac{B_1}{3}\left(1 - Bn^3\right) + \frac{1}{m^2}\left[\frac{Bn^2}{2}f^2(Bn) + Bn^2 f(Bn) - \frac{1}{2}f^2(1) - f(1)\right] \\ & + \frac{2}{m^3}\left[\frac{Bn}{6}f^3(Bn) + \frac{3Bn}{4}f^2(Bn) + Bnf(Bn) - \frac{1}{6}f^3(1) - \frac{3}{4}f^2(1) - f(1)\right] \\ & + \frac{2}{m^4}\left[\frac{1}{24}f^4(Bn) + \frac{11}{36}f^3(Bn) + \frac{7}{8}f^2(Bn) + f(Bn) - \frac{1}{24}f^4(1) - \frac{11}{36}f^3(1) - \frac{7}{8}f^2(1) - f(1)\right] \end{aligned} \tag{42}$$

For the above derivation, the following identity has been used:

$$\begin{aligned} \int\left[W(\alpha e^{\beta\xi+\delta}) + \frac{1}{2}W^2(\alpha e^{\beta\xi+\delta})\right]\xi\,d\xi = {} & \frac{1}{\beta}\left[W(\alpha e^{\beta\xi+\delta}) + \frac{3}{4}W^2(\alpha e^{\beta\xi+\delta}) + \frac{1}{6}W^3(\alpha e^{\beta\xi+\delta})\right]\xi \\ & - \frac{1}{\beta^2}\left[W(\alpha e^{\beta\xi+\delta}) + \frac{7}{8}W^2(\alpha e^{\beta\xi+\delta}) + \frac{11}{36}W^3(\alpha e^{\beta\xi+\delta}) + \frac{1}{24}W^4(\alpha e^{\beta\xi+\delta})\right] \end{aligned} \tag{43}$$

Setting $Bn = 0$ in Eq. (42) and then replacing B_1 by Bn, we obtain the volumetric flow rate for the Papanastasiou-regularized Bingham-plastic flow:

$$Q = \frac{1}{4} - \frac{Bn}{3} - \frac{1}{m^2}\left[\frac{1}{2} f^2(1) + f(1)\right] - \frac{2}{m^3}\left[\frac{1}{6} f^3(1) + \frac{3}{4} f^2(1) + f(1)\right] + \frac{2}{m^4}\left[\frac{1}{24} f^4(0) + \frac{11}{36} f^3(0) + \frac{7}{8} f^2(0) + f(0) - \frac{1}{24} f^4(1) - \frac{11}{36} f^3(1) - \frac{7}{8} f^2(1) - f(1)\right] \quad (44)$$

Dividing the velocity profile (40) by the volumetric flow rate (42), we get the normalized velocity profiles, such that the averaged velocity in the tube is unity. The normalized velocity profile for $Bn = 0.4$, $B_1 = 0.8$ and $m = 100$ is compared with its Papanastasiou ($Bn = 0$) and ideal Bingham ($Bn = B_1 = 0.8$) counterparts in Fig. 2.

Plotting the volumetric flow rate versus the regularization parameter is quite instructive. The predictions of Eq. (42) when $Bn = 0.2$ and $B_1 = 0.4$ are shown in Fig. 3. Note that fixing the values of both Bn and B_1 and increasing m is equivalent to reducing the critical shear rate $\dot{\gamma}^*$ below which the Windhab model replaces ideal viscoplastic behavior. Thus, the volumetric flow rate tends to the ideal Bingham-plastic limit (with $B_1 = 0.4$) as m goes to infinity. In the other extreme, as $m \to 0$, the trend is similar to that of the Papanastasiou model. With this model, $Bn = 0$ and the volumetric flow rate tends to the Newtonian and the Bingham-plastic limits as $m \to 0$ and ∞, respectively. The effect of the regularization parameter on the normalized velocity profiles is illustrated in Fig. 4, where results for $Bn = 0.2$, 0.4 and 0.8 and $B_1 = 2Bn$ are shown. Recall that Bn represents the dimensionless yield radius. When m is increased, the velocity profile tends to the ideal Bingham-plastic profile and this effect becomes less pronounced as Bn is increased.

3.2 Plane Poiseuille flow

Scaling lengths by the channel half-width H, stresses by GH, and the velocity by $GH^2/(2\mu)$, the dimensionless stress $\tau = |\tau_{yx}|$ and the shear rate $\dot{\gamma} = |du/dy|$ for steady pressure-driven flow between parallel plates are given by Eqs. (28) and (31), respectively. Note that G is replaced by $G/2$ and the dimensionless numbers become:

$$Bn \equiv \frac{\tau_0}{GH}, \quad B_1 \equiv \frac{\tau_1}{GH}, \text{ and } m \equiv \frac{GH}{\mu\dot{\gamma}^*} \quad (45)$$

Hence, the velocity distribution is still given by Eq. (40) with r replaced by y. However, the dimensionless volumetric flow rate is given by

$$Q = \frac{1}{3}\left(1 - Bn^3\right) - \frac{B_1}{2}\left(1 - Bn^2\right) + \frac{1}{m^2}\left[\frac{Bn}{2} f^2(Bn) + Bn f(Bn) - \frac{1}{2} f^2(1) - f(1)\right] + \frac{1}{m^3}\left[\frac{1}{6} f^3(Bn) + \frac{3}{4} f^2(Bn) + f(Bn) - \frac{1}{6} f^3(1) - \frac{3}{4} f^2(1) - f(1)\right] \quad (46)$$

Setting $Bn = 0$ in Eq. (42) and then replacing B_1 by Bn lead to the expression derived by You et al. (2008) for the Papanastasiou model:

$$Q = \frac{1}{3} - \frac{Bn}{2} - \frac{1}{m^2}\left[\frac{1}{2} f^2(1) + f(1)\right] + \frac{1}{m^3}\left[\frac{1}{6} f^3(0) + \frac{3}{4} f^2(0) + f(0) - \frac{1}{6} f^3(1) - \frac{3}{4} f^2(1) - f(1)\right] \quad (47)$$

3.3 Annular Poiseuille flow

In this section, we consider the annular Poiseuille flow of a Papanastasiou fluid in an annulus of infinite length, internal radius R_1 and external radius R_2 and denote the radii ratio R_1 / R_2 by κ ($0 < \kappa < 1$). Hence, in Eq. (31), we set $Bn = 0$ and then replace B_1 by Bn:

$$\dot{\gamma} = \frac{1}{m} W\left[mBne^{m(Bn-\tau)} \right] - Bn + \tau \tag{48}$$

The shear stress is now given by

$$\tau_{rz} = \frac{c}{r} - \frac{G}{2} r \tag{49}$$

where c/r is the homogeneous solution and $-Gr/2$ is the particular solution. The shear stress is positive in (κ, R) (Region I), as is the shear rate du/dr. In $(R,1)$ (Region II) both are negative. Let R be the radius where the velocity attains its maximum and thus the shear stress vanishes, $\tau_{rz}(R) = 0$. Then we see that $c = R^2/2$ and thus

$$\tau_{rz} = \frac{G}{2}\left(\frac{R^2}{r} - r \right) \tag{50}$$

With the scales introduced in this section, the dimensionless version of Eq. (50) is

$$\tau_{rz} = \frac{R^2}{r} - r \tag{51}$$

Therefore, from Eq. (48) we have for the velocity derivatives

$$\left.\frac{du}{dr}\right|_I = \frac{1}{m} W\left[mBne^{m\left(Bn - R^2/r + r\right)} \right] - Bn + \frac{R^2}{r} - r \tag{52}$$

and

$$\left.\frac{du}{dr}\right|_{II} = -\frac{1}{m} W\left[mBne^{m\left(Bn + R^2/r - r\right)} \right] + Bn + \frac{R^2}{r} - r \tag{53}$$

in regions I and II, respectively. Integrating the velocity derivatives in both regions and applying the no-slip boundary condition at the two cylinders, one gets the velocity profile:

$$u(r) = \begin{cases} \int_\kappa^r \left(du/d\xi\right)_I \, d\xi, & \kappa \le r \le R \\ \int_r^1 \left(du/d\xi\right)_{II} \, d\xi, & R \le r \le 1 \end{cases} \tag{54}$$

The radius R is determined by demanding that $u_I(R) = u_{II}(R)$ which leads to

$$\frac{1}{m}\int_\kappa^R W\left[mBne^{m\left(Bn - R^2/\xi + \xi\right)} \right] d\xi - \frac{1}{m}\int_R^1 W\left[mBne^{m\left(Bn + R^2/\xi - \xi\right)} \right] d\xi = R^2 \ln\frac{R^2}{\kappa} - \frac{1-\kappa}{2}\left(1 + \kappa + Bn\right) \tag{55}$$

Once R is calculated be solving Eq. (55), the velocity profile can be computed by means of Eq. (54).

Recall that in ideal Bingham-plastic flow (Bird et al., 1983), the material is unyielded between r_I and r_{II} in regions I and II, respectively, such that $|\tau_{rz}| = Bn$. Thus, from Eq. (51) we find

$$\frac{R^2}{r_I} - r_I = -\frac{R^2}{r_{II}} + r_{II} = Bn \tag{56}$$

from which the two critical radii can easily be calculated as functions of the Bingham number. It turns out that $r_{II} - r_I = Bn$, from which it is deduced that there is no flow when $Bn \ge Bn_c = 1 - \kappa$. In Figs. 5 and 6 we show velocity profiles obtained for various values of the Bingham number and the parameter m and $\kappa = 0.5$ and 0.2, respectively. It can be observed that moderate values of m yield satisfactory results only for big values of

the ratio κ and low Bingham numbers. The deviations from the ideal Bingham-plastic solutions, where the velocity profile in the unyielded region is flat, become more pronounced as the Bingham number is increased and tends to the critical value $Bn_c = 1-\kappa$. Much higher values of m should be used in order to approximate satisfactorily the velocity profiles of an ideal Bingham plastic.

4. Viscoelastic flows

The Lambert W function is also encountered in viscoelastic flows. Here, we briefly describe a solution for a PTT fluid flow first reported by Ferrás et al. (2012). The tensorial form of the PTT constitutive equation is given by (Phan-Thien and Tanner, 1977):

$$g(tr\boldsymbol{\tau})\,\boldsymbol{\tau} + \lambda \overset{\nabla}{\boldsymbol{\tau}} = 2\eta \mathbf{D} \tag{57}$$

where λ is the relaxation time, ε a parameter related to the elongational behaviour of the fluid and η is the constant shear viscosity. The symbol $\overset{\nabla}{\boldsymbol{\tau}}$ denotes Oldroyd's upper-convected derivative of the stress tensor:

$$\overset{\nabla}{\boldsymbol{\tau}} = \frac{D\boldsymbol{\tau}}{dt} - \boldsymbol{\tau}\cdot\nabla\mathbf{u} - \left(\nabla\mathbf{u}\right)^T\cdot\boldsymbol{\tau} \tag{58}$$

where $D\cdot/dt$ is the material derivative operator. Of interest here is the exponential form of the model where (Phan Thien, 1978)

$$g(tr\boldsymbol{\tau}) = e^{\varepsilon\lambda\, tr\boldsymbol{\tau}/\eta} \tag{59}$$

Consider the steady-state plane Couette flow between infinite parallel plates separated by a distance H with the upper plate moving in the x-direction at a constant velocity V while the lower plate is stationary. In this unidirectional flow, $u = u(y)$ and the only non-zero components of the stress tensor are τ_{xx} and τ_{yx}. The corresponding components of Eq. (57) are

$$\left.\begin{aligned} g(\tau_{xx})\tau_{xx} &= 2\lambda\tau_{yx}\frac{du}{dy} \\ g(\tau_{xx})\tau_{yx} &= \eta\frac{du}{dy} \end{aligned}\right\} \tag{60}$$

from which one gets

$$\tau_{xx} = \frac{2\lambda}{\eta}\tau_{yx}^2 \tag{61}$$

and therefore

$$\tau_{yx} e^{2\varepsilon\lambda^2\tau_{yx}^2/\eta^2} = \eta\frac{du}{dy} \tag{62}$$

In the case of no slip, $du/dy = V/H$. Equation (62) can be written in the form (2) and then can be solved for τ_{yx}^2, yielding the following expression derived by Ferrás et al. (2012) for the shear stress required to move the upper plate at a constant velocity V:

$$\tau_{yx} = \frac{\eta}{2\lambda}\sqrt{\frac{1}{\varepsilon}W\left(\frac{4\varepsilon\lambda^2V^2}{H^2}\right)} \tag{63}$$

5. Wall slip with non-zero slip yield stress

In this section, we solve two flow problems with wall slip and non-zero slip yield stress by adopting the regularized slip equation (11) and making use of the Lambert function. More specifically, we consider the axisymmetric Poiseuille flow of a power-law fluid and the circular Couette flow of a Newtonian fluid.

5.1 Axisymmetric Poiseuille flow with wall slip

We consider the Poiseuille flow of a power-law fluid in a tube of radius R with wall slip obeying Eq. (10). The constitutive equation reads:

$$\tau = k\dot{\gamma}^n \tag{64}$$

where k is the consistency index and n is the exponent. From Eq. (26), the wall shear stress is $\tau_w = |\tau_{rz}|_{r=R} = GR/2$ and thus slip occurs above the critical pressure gradient $G_c = 2\tau_c / R$ at which the wall shear stress is equal to the slip yield stress, $\tau_w = \tau_c$. One then needs to consider separately the solutions below and above the critical pressure gradient G_c. We will work with dimensionless parameters, scaling lengths by R, stresses by the slip yield stress τ_c, the pressure gradient by τ_c / R, and the velocity by $\tau_c^{1/n} R / k^{1/n}$. With these scalings, the dimensionless critical pressure gradient is $G_c = 2$ and the dimensionless velocity is given by

$$u(r) = u_w + \frac{G^{1/n}}{2^{1/n}(1+1/n)}\left(1 - r^{1/n+1}\right) \tag{65}$$

where

$$u_w = \begin{cases} 0, & G \le 2 \\ B\left(G/2 - 1\right), & G > 2 \end{cases} \tag{66}$$

and

$$B \equiv \frac{k^{1/n}}{\tau_c^{1/n-1} R\beta} \tag{67}$$

is the slip number. When $n = 1$, Eq. (65) is reduced to the Newtonian solution derived by Kaoullas et al. (2013).

The advantage of the regularized slip equation (11) is that it applies for all the values of the pressure gradient. Given that the dimensionless wall shear stress is $\tau_w = G/2$, the dimensionless version of Eq. (12) for the slip velocity is

$$u_w = B\left(G/2 - 1\right) + \frac{1}{M_c} W\left[M_c B e^{-M_c B(G/2-1)}\right] \tag{68}$$

where

$$M_c \equiv \frac{m_c \tau_c^{1/n} R}{k^{1/n}} \tag{69}$$

Equation (68) provides a good estimate of the slip velocity in and near the no-slip regime only for sufficiently large values of M_c. This is illustrated in Fig. 7 where results for $B = 0.1$ (weak slip) and 1 (strong slip) are shown.

5.2 Circular Couette flow with wall slip

Consider now the Newtonian flow between long coaxial cylinders under the assumption that slip occurs only along the inner, rotating cylinder following the two-branch slip equation (10). Recall that in the general case the steady-state solution is of the form (Papanastasiou et al., 1999)

$$u_\theta(r) = c_1 r + \frac{c_2}{r} \text{ and } \tau_{r\theta}(r) = -2\eta \frac{c_2}{r^2} \tag{70}$$

where the constants c_1 and c_2 are determined from the boundary conditions. It is clear that no-slip is observed below the critical angular velocity Ω_c at which the inner wall shear stress is equal to the slip yield stress, $\tau_w = \tau_c$. Therefore, for $\Omega \le \Omega_c$ the boundary conditions read $u_\theta(\kappa R_2) = \Omega \kappa R_2$ and $u_\theta(R_2) = 0$, where, as in Section 3.3, $\kappa \equiv R_1 / R_2$. Thus, one gets the standard no-slip solution

$$u_\theta(r) = \frac{\kappa^2 \Omega r}{1-\kappa^2}\left(\frac{R_2^2}{r^2} - 1\right) \quad \text{and} \quad \tau_{r\theta}(r) = -\frac{2\eta\kappa^2 R_2^2 \Omega}{(1-\kappa^2) r^2} \tag{71}$$

Since $\tau_w = \left|\tau_{r\theta}(\kappa R_2)\right|$, the critical angular velocity is given by

$$\Omega_c \equiv \frac{(1-\kappa^2)\tau_c}{2\eta} \tag{72}$$

Above this critical value, slip occurs along the inner cylinder and the boundary condition along the inner cylinder becomes $u_\theta(\kappa R_2) = \Omega \kappa R_2 - u_w$, where the slip velocity u_w satisfies the slip law (10). It turns out that

$$u_w = \frac{\kappa R_2 (\Omega - \Omega_c)}{1+B} \tag{73}$$

and the azimuthal velocity is given by

$$u_\theta(r) = \frac{(B\Omega + \Omega_c)\kappa^2 r}{(1+B)(1-\kappa^2)}\left(\frac{R_2^2}{r^2} - 1\right) \tag{74}$$

where

$$B \equiv \frac{\beta\kappa(1-\kappa^2)R_2}{2\eta} \tag{75}$$

is the slip number for this flow. In summary the velocity is given by equations (71) or (74), depending on whether Ω is below or above the critical value Ω_c. For the slip velocity we can write:

$$u_w = \begin{cases} 0, & \Omega \le \Omega_c \\ \dfrac{(\Omega - \Omega_c)\kappa R_2}{1+B}, & \Omega > \Omega_c \end{cases} \tag{76}$$

The need of considering the different flow regimes is eliminated when using the regularized slip equation (11). From the boundary conditions and the latter equation, one finds that the slip velocity satisfies the following equation:

$$-M_c \frac{u_w}{\Omega_c \kappa R_2} = \ln\left[1 - \frac{\Omega}{\Omega_c} + (1+B)\frac{u_w}{\Omega_c \kappa R_2}\right] \tag{77}$$

where M_c is now defined by

$$M_c \equiv m_c \Omega_c \kappa R_2 \tag{78}$$

Equation (77) is of the form (4) and therefore it is solved for the slip velocity by means of the Lambert function:

$$\frac{u_w}{\Omega_c \kappa R_2} = \frac{\Omega/\Omega_c - 1}{1+B} - \frac{1}{M_c} W\left[\frac{M_c}{1+B} e^{-\frac{M_c}{1+B}(\Omega/\Omega_c - 1)}\right] \tag{79}$$

which holds for any value of the angular velocity Ω. Finally, the velocity is given by

$$u_\theta(r) = \left\{\frac{B\Omega + \Omega_c}{1+B} - \frac{\Omega_c}{M_c} W\left[\frac{M_c}{1+B} e^{-\frac{M_c}{1+B}(\Omega/\Omega_c - 1)}\right]\right\} \frac{\kappa^2 r}{1-\kappa^2}\left(\frac{R_2^2}{r^2} - 1\right) \tag{80}$$

For high values of the regularization parameter M_c, Eq. (79) approximates the behavior of the two-branch Eq. (76). Plotting the slip velocity versus the angular velocity for various values of M_c results in graphs very similar to those of Fig. 6.

6. Conclusions

We have derived analytical solutions for various non-Newtonian flows in terms of Lambert's W function. Explicit expressions for the radii of the yielded regions are provided for the circular and annular Couette flows of a Bingham plastic. The analytical solutions of You et al. (2008) for the plane and round Poiseuille flows of a fluid obeying the Papanastasiou regularization for the Bingham plastic have been extended to the annular Poiseuille flow and also to Windhab fluids. For completeness, the solution of Ferrás et al. (2012) for the shear stress in plane Couette flow of an exponential Phan-Thien-Tanner fluid has been included. Finally, we have pointed out that the Lambert function can be used when using a regularized slip equation with non-zero slip yield stress in order to obtain solutions that hold in all the flow regimes. This idea has been applied to solve the axisymmetric Poiseuille flow of a power-law fluid and the Newtonian circular Couette flow.

In all the solutions presented here the primary branch of the Lambert function, $W_0(x)$ is used with a positive argument. The only exception in the circular Couette flow of a Bingham plastic where the radius of the yielded region is expressed in terms of the secondary branch $W_{-1}(x)$ of the Lambert function, which is defined in $[-1/e, 0)$.

Data availability

The data that support the findings of this study are available from the corresponding author upon reasonable request.

References

1. A.N. Alexandrou, G.C. Florides, G.C. Georgiou, Squeeze flow of semi-solid slurries, J. Non-Newtonian Fluid Mech. 193, 103-115 (2013).
2. N.J. Balmforth, I.A. Frigaard, G. Ovarlez, Yielding to stress: Recent developments in viscoplastic fluid mechanics, Annu. Rev. Fluid Mech. 46, 121-46 (2014).
3. P. Ballesta, G. Petekidis, L. Isa, W.C.K. Poon, R. Besseling, Wall slip and flow of concentrated hard-sphere colloidal suspensions. J. Rheol. 56, 1005-1037 (2012).
4. Bingham EC (1922) Fluidity and Plasticity. McGraw Hill, New-York.
5. R.B. Bird, G. Dai, B.J. Yarusso, The rheology and flow of viscoplastic materials, Rev. Chem. Eng. 1, 1-70 (1983).
6. D. Bonn, J. Paredes, M.M. Denn, L. Berthier, T. Divoux, S. Manneville, Yield stress materials in soft condensed matter, Rev. Mod. Phys. 89, 035005 (2017).
7. R.M. Corless, G.H. Gonnet, D.A. Hare, D.J. Jeffrey, D.E. Knuth, On the Lambert W function, Advances in Computational Mathematics 5, 329-359 (1996).
8. Y. Damianou, M. Philippou, G. Kaoullas, G.C. Georgiou, Cessation of viscoplastic Poiseuille flow with wall slip, J. Non-Newtonian Fluid Mech. 203, 24-37 (2014).
9. Y. Damianou, G. Kaoullas, G.C. Georgiou, Cessation of viscoplastic Poiseuille flow in a square duct with wall slip, J. Non-Newtonian Fluid Mech. 233, 13-26 (2016).
10. Y. Damianou, P. Panaseti, G.C. Georgiou, Viscoplastic Couette flow in the presence of wall slip with non-zero slip yield stress, Materials 12(21), 3574 (2019).
11. P.-G. de Gennes, on fluid/wall slippage, Langmuir 18, 3413-3414 (2002).

12. J. Férec, E. Bertevas, B. Cheong Khoo, G. Ausias, N. Phan-Thien, A rheological constitutive model for semiconcentrated rod suspensions in Bingham fluids, Phys. Fluids 29, 073103 (2017).
13. L.L. Ferrás, J.M. Nóbrega, F.T. Pinho, Analytical solutions for channel flows of Phan-Thien-Tanner and Giesekus fluids under slip, J. Non-Newtonian Fluid Mech. 171-172, 97-105 (2012).
14. L.O. Figura, A.A. Texeira, Food Physics, Physical Properties - Measurement and Applications, Springer-Verlag, Berlin-Heidelberg, 2007.
15. I. Frigaard, Simple yield-stress fluids. Curr. Opinion Coll. Inter. Sci. 43: 80-93, 2019.
16. V. Glicerina, F. Balestra, M. Dalla Rosa, S. Romani, Microstructural and rheological characteristics of dark, milk, and white chocolate: A comparative study, J. Food Eng. 169, 165-171 (2016).
17. G. Kaoullas, G.C. Georgiou, Newtonian Poiseuille flows with wall slip and non-zero slip yield stress, J. Non-Newtonian Fluid Mech. 197, 24-30 (2013).
18. A.Y. Malkin; S.A. Patlazhan, Wall slip for complex fluids – Phenomenon and its causes, Adv. Colloid Interface Sci. 257, 42-57 (2018).
19. S.P. Meeker, R.T. Bonnecaze, M. Cloitre, Slip and flow in soft particle pastes, Phys. Rev. Let. 92, 198302 (2004).
20. C.L.M.H. Navier, Sur les lois du mouvement des fluids. Mem. Acad. R. Sci. Inst. Fr. 389-440 (1827).
21. T.C. Papanastasiou, Flows of materials with yield, J. Rheology 31, 385-404 (1987).
22. T. Papanastasiou, G. Georgiou and A. Alexandrou, Viscous Fluid Flow, CRC Press, Boca Raton, 2000.
23. N. Phan-Thien, R.I. Tanner, A new constitutive equation derived from network theory, J. Non-Newtonian Fluid Mech. 2, 353-365 (1977).
24. N. Phan-Thien, A nonlinear network viscoelastic model, J. Rheol. 22, 259-283 (1978).
25. J.M. Piau, Carbopol gels: Elastoviscoplastic and slippery glasses made of individual swollen sponges: Meso- and macroscopic properties, constitutive equations and scaling laws, J. non-Newtonian Fluid Mech. 144, 1-29 (2007)
26. R. Pitsillou, A. Syrakos, G.C. Georgiou, Application of the Lambert W function to steady shearing Newtonian flows with logarithmic wall slip, Physics of Fluids 32, 053107 (2020).
27. T. Sochi, Slip at fluid-solid interface, Polymer Reviews 51, 309-340 (2011).
28. H. Spikes; S. Granick, Equation for slip of simple liquids at smooth solid surfaces, Langmuir 19, 5065-5071 (2003).
29. A. Syrakos, Y. Dimakopoulos, G.C. Georgiou, J. Tsamopoulos, Viscoplastic flow in an extrusion damper, J. Non-Newtonian Fluid Mech. 232, 102-124 (2016).
30. Z. You, R.R. Huilgol, E. Mitsoulis, Application of the Lambert W function to steady shearing flows of the Papanastasiou model, Int. J. Eng. Sci. 46, 799-808 (2008).

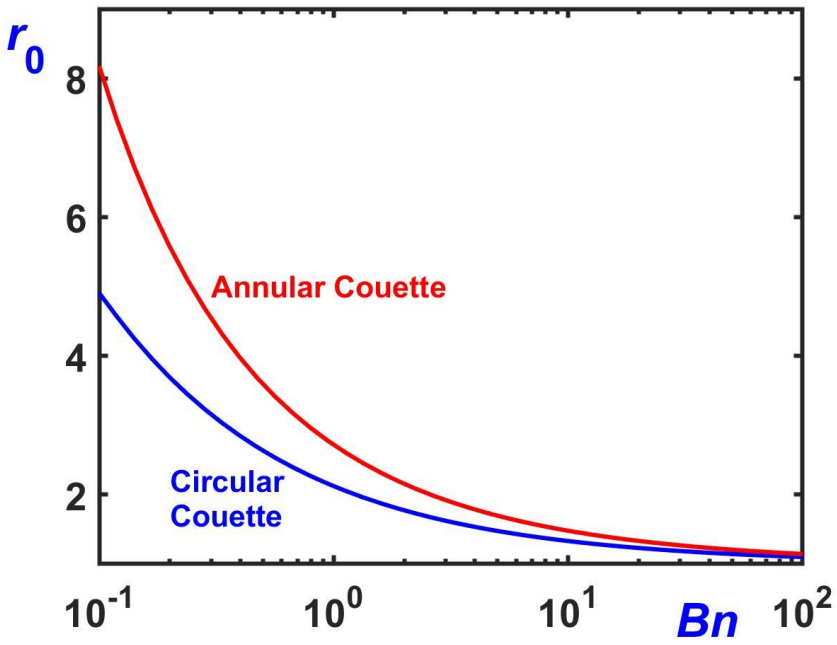

Figure 1. Yield radii in circular and annular Couette flows as functions of the corresponding Bingham number via Eqs. (17) and (22), respectively.

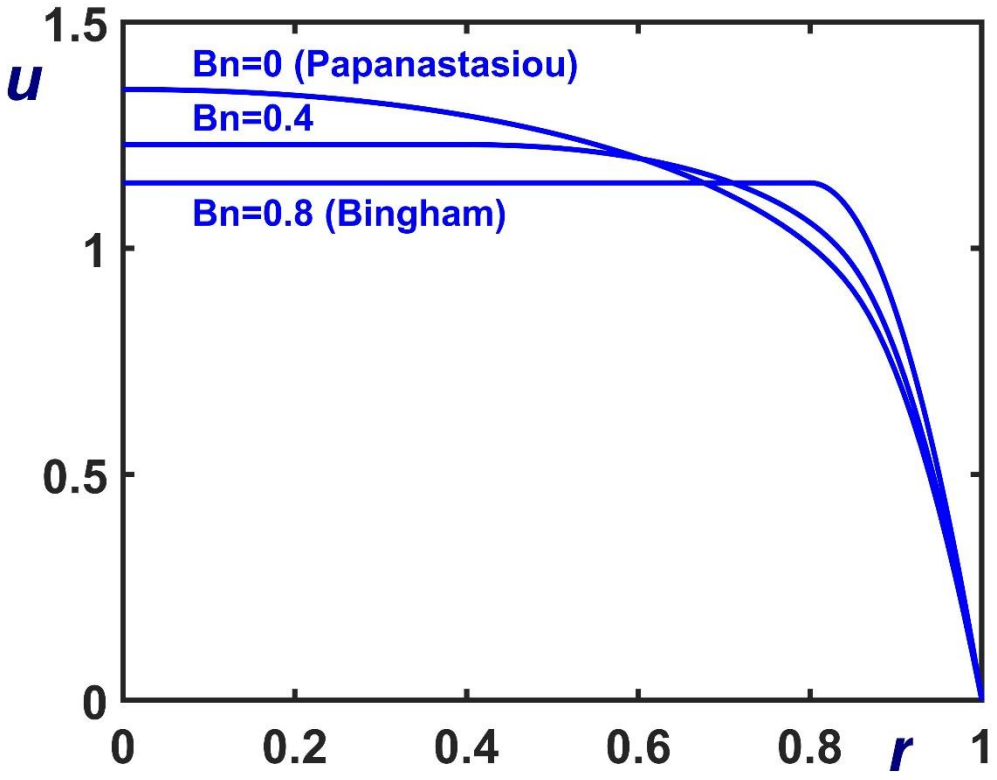

Figure 2. Normalized velocity profile in axisymmetric Poiseuille flow of a Windhab fluid with $m = 100$, $Bn = 0.4$ and $B_1 = 0.8$ compared with the corresponding Papanastasiou ($Bn = 0$) and ideal Bingham ($Bn = B_1 = 0.8$) profiles.

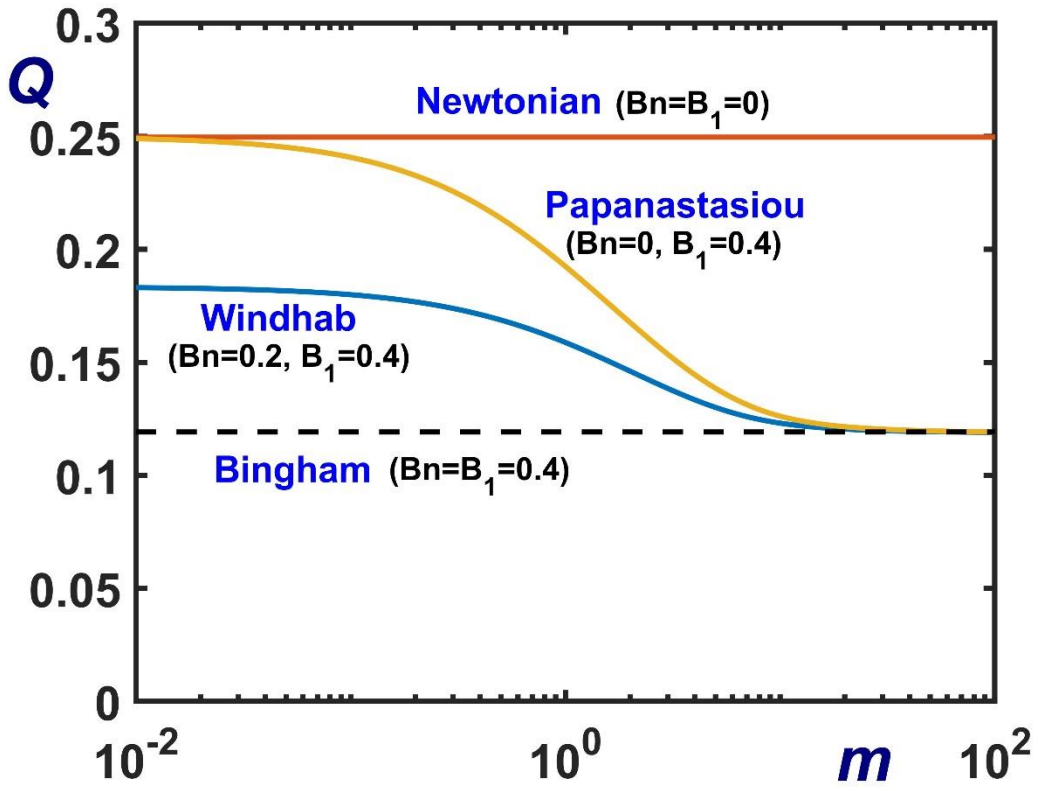

Figure 3. Dimensionless volumetric flow rate versus the regularization parameter in axisymmetric Poiseuille flow of a Windhab fluid with $Bn = 0.2$ and $B_1 = 0.4$ and a Papanastasiou fluid with $Bn = 0$ and $B_1 = 0.4$. The two curves are bounded by the Newtonian ($Bn = B_1 = 0$) and the ideal Bingham-plastic ($Bn = B_1 = 0.4$) limits.

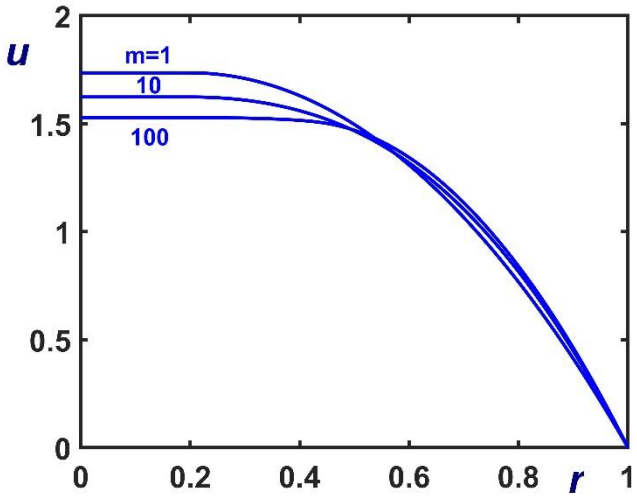

(a)

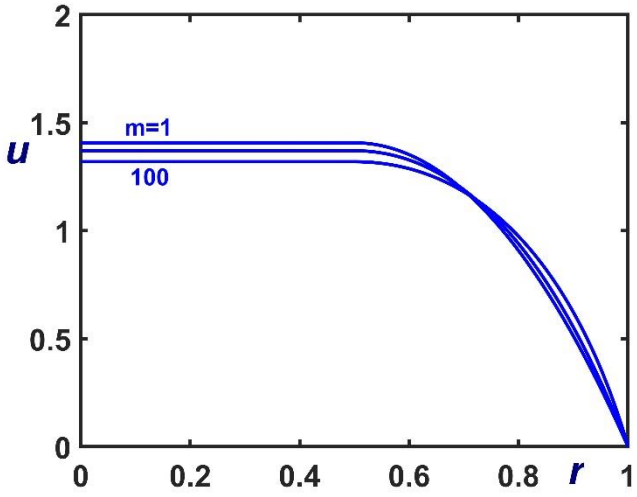

(b)

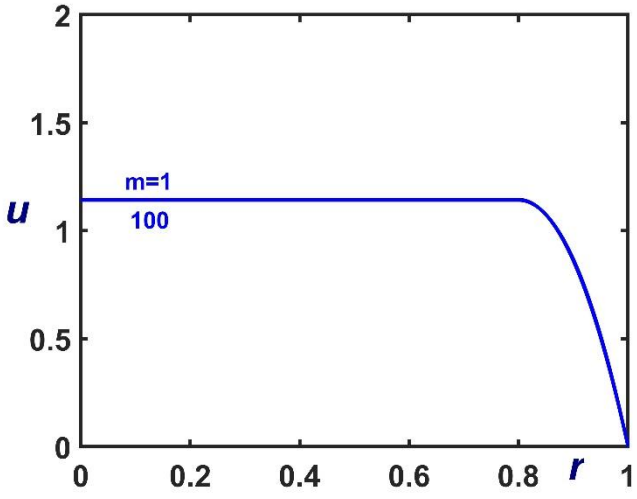

(c)

Figure 4. Normalized velocity profiles in axisymmetric Poiseuille flow of a Windhab fluid for various values of the dimensionless parameter m: (a) $Bn = 0.2$ and $B_1 = 0.4$; (b) $Bn = 0.5$ and $B_1 = 1$; (c) $Bn = 0.8$ and $B_1 = 1.6$.

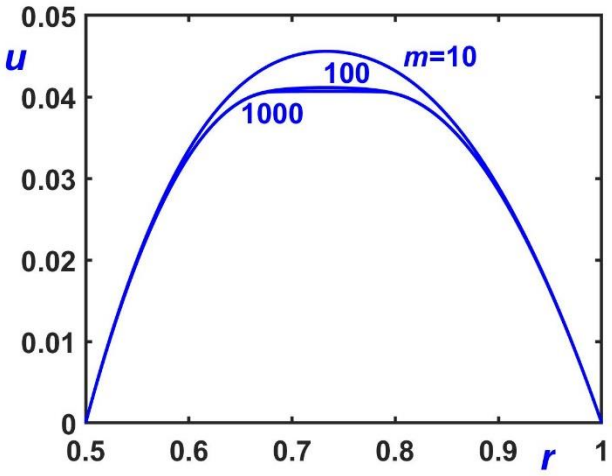

(a)

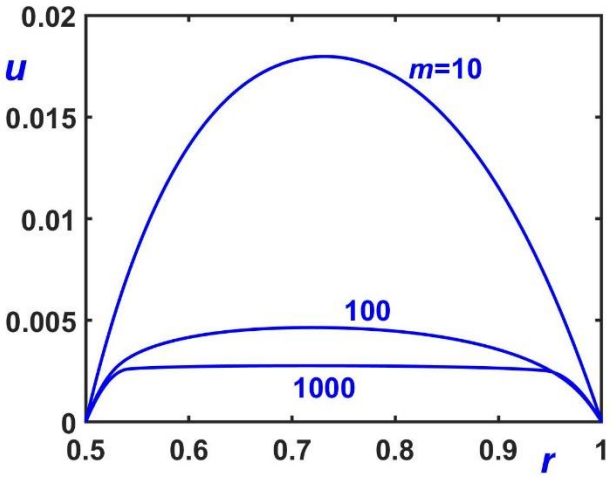

(b)

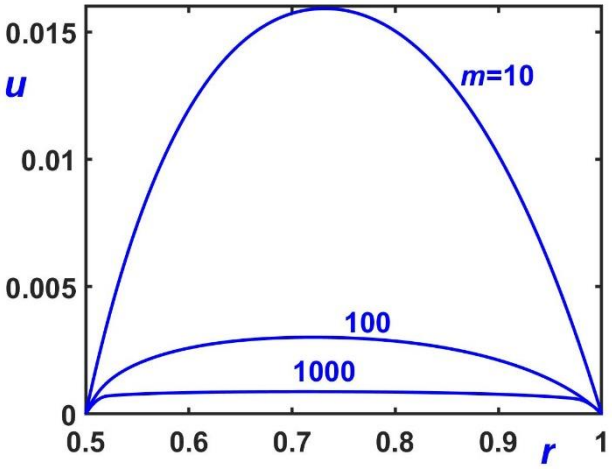

(c)

Figure 5. Effect of the regularization parameter on the velocity profile in pressure-driven flow of a Papanastasiou-regularized Bingham plastic fluid in an annulus with radii ratio $\kappa = 0.5$: (a) $Bn = 0.2$; b) $Bn = 0.4$; c) $Bn = 0.45$.

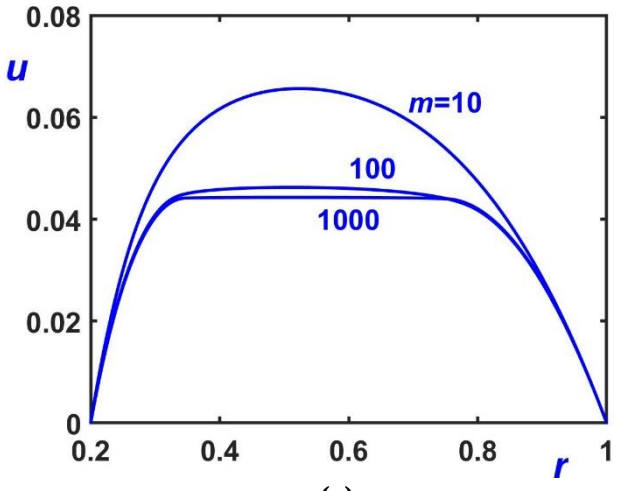

(a)

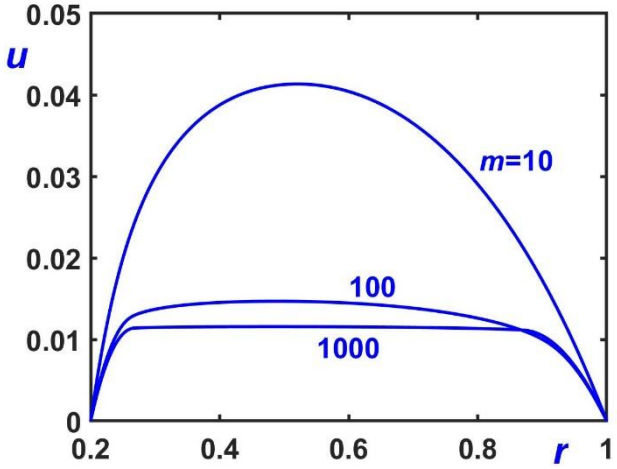

(b)

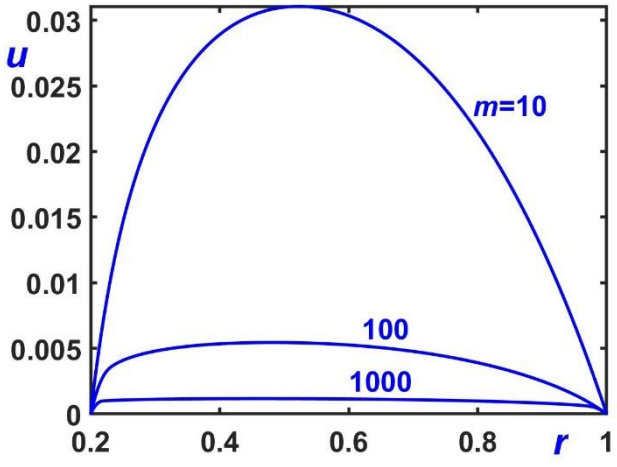

(c)

Figure 6. Effect of the regularization parameter on the velocity profile in pressure-driven flow of a Papanastasiou-regularized Bingham plastic fluid in an annulus with radii ratio $\kappa = 0.2$: (a) $Bn = 0.2$; b) $Bn = 0.4$; c) $Bn = 0.45$.

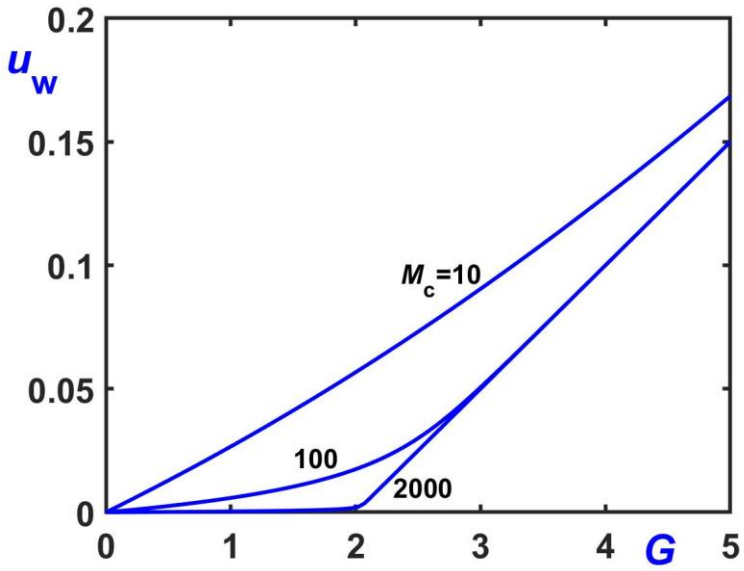

(a)

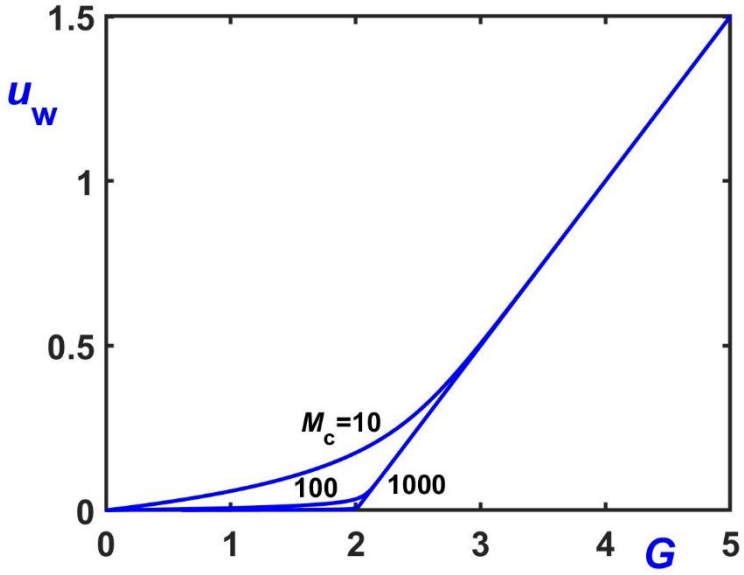

(b)

Figure 7. Slip velocity in axisymmetric Poiseuille flow with wall slip and non-zero slip yield stress for various values of the regularization parameter M_c: (a) $B = 0.1$ (weak slip); (b) $B = 1$ (strong slip).